

# SideEye: A Generative Neural Network Based Simulator of Human Peripheral Vision

Lex Fridman  
MIT

Bryan Reimer  
MIT

Benedikt Jenik  
MIT

Christoph Zetsche  
University of Bremen

Shaiyan Keshvari  
MIT

Ruth Rosenholtz  
MIT



(a) Looking at the GPS navigation screen in the center stack.



(b) Looking at the pedestrian.

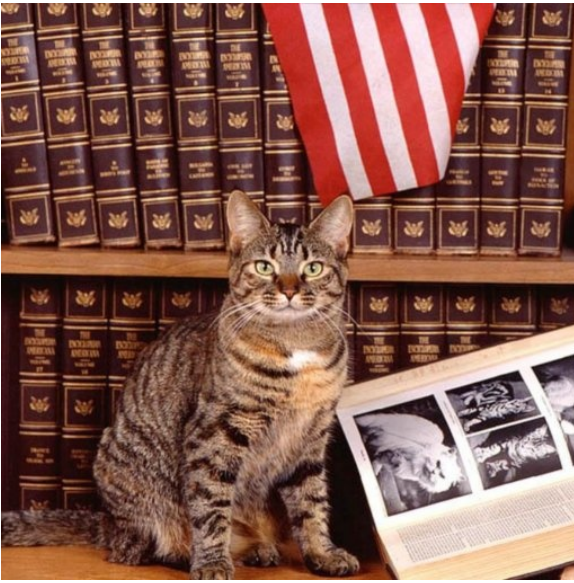
Figure 1: Peripheral vision simulation using a generative neural network trained on a behaviorally-validated model of human peripheral vision. Our SideEye tool uses this model to simulate what an observer sees when foveating the location of the mouse pointer. Note: In the figure on the left, when looking at the center stack, the pedestrian is not visible in the periphery.

## ABSTRACT

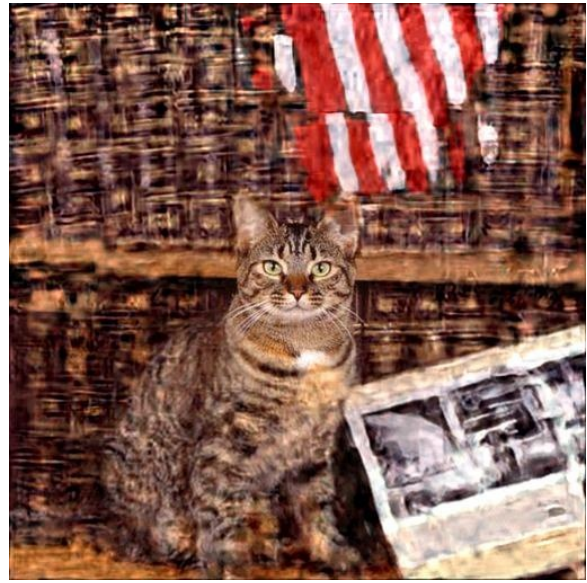
Foveal vision makes up less than 1% of the visual field. The other 99% is peripheral vision. Precisely what human beings see in the periphery is both obvious and mysterious in that we see it with our own eyes but can't visualize what we see, except in controlled lab experiments. Degradation of information in the periphery is far more complex than what might be mimicked with a radial blur. Rather, behaviorally-validated models hypothesize that peripheral vision measures a large number of local texture statistics in pooling regions that overlap and grow with eccentricity. In this work, we develop a new method for peripheral vision simulation by training a generative neural network on a behaviorally-validated full-field synthesis model. By achieving a 21,000 fold reduction in running time, our approach is the first to combine realism and speed of peripheral vision simulation to a degree that provides a whole new way to approach visual design: through peripheral visualization.

## INTRODUCTION AND RELATED WORK

In the fovea (the central rod-free area of the retina, approximately  $1.7^\circ$  in diameter), recognition is relatively robust and effortless. However, more than 99% of visual field lies outside the fovea, here referred to as the periphery. Peripheral vision has considerable loss of information relative to the fovea. This begins at the retina, which employs variable spatial resolution to get past the bottleneck of the optic nerve. However, it does not end there, but continues with neural operations in visual cortex. Reduced peripheral acuity has only a tiny effect, compared with peripheral vision's sensitivity to clutter, known as visual crowding (discussed in more detail in the "Crowding in Peripheral Vision" section). Unlike acuity losses, which impact only tasks relying on quite high spatial frequencies, crowding occurs with a broad range of stimuli [20]. It is ever-present in real-world vision, in which the visual system is faced with cluttered scenes full of objects and diverse textures. Crowding constrains what we can perceive at a glance.



(a) Original  $512 \times 512$  pixel image.



(b) Foveated image with fixation on (256, 256).

Figure 2: Example “foveated” image. Given an original image (a), the foveated image provides a visualization of the information available from a single glance (b) assuming the two subfigures are 14.2 inches away from the observer on a printed page (2.6 inches in height and width) and the observer’s eyes are fixated at the center of the original image. By selecting a new model fixation, one can similarly get predictions for that fixation. Any part of the image that appears clearly in (b) is predicted to be easy to perceive when fixating at the center of (a). The stripes in the flag are clear. The cat is clearly identifiable as such, and clearly sits next to a book. The pictures within the book are not predicted to have a clear organization, given the modeled fixation. The image in this example comes from the dataset used in the paper.

The field of human vision has recently made significant advances in understanding and modeling peripheral vision. A successful model has been shown to predict performance at a number of peripheral and full-field vision tasks [2, 8, 12, 27, 34]. Critically, from the point of view of converting this understanding to design intuitions, researchers have visualized both reduced acuity and visual crowding using foveated texture synthesis techniques that generate new image samples that have the same texture statistics in a large number of overlapping “pooling” regions [8, 26]. Such visualizations facilitate intuitions about peripheral vision, e.g. for design [23], and also enable testing models of peripheral vision. However, generating each synthesis can take a number of hours, limiting the utility of this technique.

In this work, we develop and release a Foveated Generative Network (FGN) architecture for end-to-end learning of the foveation task and an online tool (SideEye) for real-time simulation of peripheral vision on user-submitted designs. The primary goal of this approach is to reduce the running time of generating a human-realistic visualization of peripheral vision from hours to milliseconds while maintaining reasonable consistency with the behaviorally validated models. Fig. 2 shows an example visualizing the degradation of spatial information in the periphery. Being able to perform a visualization like this in under a second has several significant applications (see list below). As discussed in the “Running Time Performance” section, the average running time of 700 ms could be

further significantly reduced. As it approaches 33 ms (or 30 fps), the following applications become even more feasible:

- **Interface Design:** Explore various graphic user interface design options with the SideEye tool on the fly by adjusting the fixation point and visualizing the full-field appearance of the design given the fixation point in near real-time (see Fig. 1). One example of this application is the A/B testing of website designs [10]. An illustrative case study of this testing-based design methodology is presented in the the “Application Case Study: A/B Testing of Design Layouts” section. Communicate design intuitions and rationale to members of the design or product team.
- **Insights into Usability and Safety:** Quickly gain intuitions about HCI issues such as whether, in an automotive context, a user is likely to notice obstacles (i.e., pedestrians) while engaged with a cell phone, GPS system, or augmented reality headset. An example of this type of exploration using the SideEye tool is shown in Fig. 1.
- **Behavioral Evaluation of Vision Model on HCI-relevant stimuli and tasks:** The existing peripheral vision model has been extensively tested on a wide range of stimuli and tasks, providing confidence that the model extends to HCI-relevant visual tasks. Nonetheless, additional testing is always desirable. Previous model testing has utilized peripheral vision visualizations to generate model predictions (see, e.g. [34], for the standard methodology). For HCI tasks, this requires generating hundreds

of foveated images dependent on subject fixation patterns. FGN can generate the needed set of foveated images on-the-fly as the subject is performing the experiment.

- **Video Foveation:** Fast image foveation can be applied to individual frames of a video. This is an important step toward producing a model of peripheral vision in real-world viewing. However, there are further modeling challenges like accounting for peripheral encoding of motion and maintaining temporal consistency would need to be added to the architecture in order to make video foveation a powerful tool to explore human processing of spatiotemporal visual information.

The main contribution of this work is to use a deep learning approach to make a model of human vision fast enough to provide a useful design tool. This will facilitate more effective communication of visual information, better usability, early insight into performance of a given design prior to user testing, and better communication within the design team [25]. To further use of this tool, we release the code and an online in-browser version at [https://\\*\\*\\*\\*.\\*\\*\\*.\\*\\*\\*/peripheral](https://****.***.***/peripheral). We demonstrate that the resulting model successfully approximates the state-of-the-art behaviorally validated model, and yet is 21,000 times faster.

## MODELING PERIPHERAL VISION

### Crowding in Peripheral Vision

It is well known that the visual system has trouble recognizing peripheral objects in the presence of nearby flanking stimuli, a phenomenon known as crowding (for reviews see: [15, 20, 31]). Fig. 4 shows a classic demonstration. Fixating the central cross, one can likely easily identify the isolated ‘A’ on the left but not the one on the right flanked by additional letters. An observer might see these crowded letters in the wrong order, e.g., ‘BORAD’. They might not see an ‘A’ at all, or might see strange letter-like shapes made up of a mixture of parts from several letters [14]. Move the flanking letters farther from the target ‘A’, and at a certain critical spacing recognition is restored. The critical spacing is approximately 0.4 to 0.5 times the eccentricity (the distance from the center of fixation to the target) for a fairly wide range of stimuli and tasks [3, 18, 19]. Authors in [20] have dubbed this *Bouma’s Law*.

It should be clear that such “jumbling” in the periphery has profound consequences for HCI design. In fact, crowding is likely task-relevant for most real-world visual stimuli and tasks. It has a far greater impact on vision than loss of acuity or color vision, and it is the dominant difference between foveal and peripheral vision [24]. It impacts visual search, object recognition, scene perception, perceptual grouping, shape perception, and reading [20, 26, 27]. Crowding demonstrates a tradeoff in peripheral vision, in which significant information about the visual details is lost, and yet considerable information remains to support many real-world visual tasks and to give us a rich percept of the world. The information that survives must suffice to guide eye movements and give us a coherent view of the visual world [22]. Nonetheless, the pervasive loss of information throughout the visual

field means that we cannot hope to understand much of vision without understanding, controlling for, or otherwise accounting for the mechanisms of visual crowding.

A fair assessment of the current state of vision research is that there exists a dominant theory of crowding. Crowding has been equivalently attributed to “excessive or faulty feature integration”, “compulsory averaging”, or “forced texture processing” “pooling”, resulting from features over regions that grow linearly with eccentricity [2, 14, 15, 17, 20]. Pooling has typically been taken to mean averaging [17] or otherwise computing summary statistics [2, 14] of features within the local region.

### A Statistical Model

Authors in [2] operationalized earlier theories of statistical processing in peripheral vision [14, 17] in terms of measurement of a rich set of texture statistics within local pooling regions that grow linearly with eccentricity, in accord with Bouma’s Law. They used as their candidate statistics those identified by authors in [21], as that set has been successful at describing texture perception (as judged by synthesis of textures that are difficult to discriminate from the original). Authors in [8] generalized this model to synthesize images from local texture statistics computed across the field of view, often referred to as the “V2 model”, as they suggested that these computations might occur in visual processing area V2 in the brain. Authors in [26] have similarly developed full-field synthesis techniques, and refer to the full model as the Texture Tiling Model (TTM).

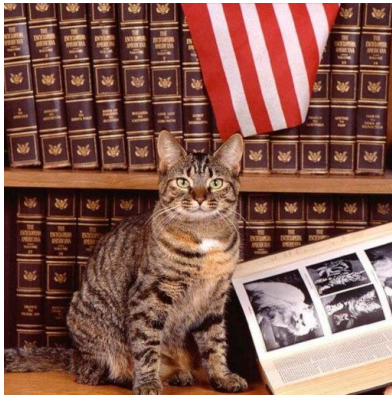
Fig. 3 shows four examples of foveated images generated by TTM. Note that because of the statistical nature of the model, each input image corresponds to a large number of output images that share the same texture statistics. Critically, these synthesized model images aid intuitions about what visual tasks will be easy to perform at a glance, i.e. with the information available in the periphery plus the high resolution fovea. Regions of the synthesized image that appear clear are well represented by peripheral vision, according to the model. Tasks that are easy to perform with the synthesized images will be easy to perform at a glance. For instance, the model predicts that it is obvious at a glance that the first image in the figure is of a cat, sitting amongst books and below a flag. However, the layout and content of the open book may be difficult to discern.

The V2 model and TTM [8, 26] share many features, including the local texture statistics, and overlapping pooling regions that overlap and grow linearly with eccentricity. This paper utilizes the TTM synthesis procedure, so we adopt that terminology.

Mounting evidence supports TTM as a good candidate model for the peripheral encoding underlying crowding; it predicts human performance at peripheral recognition tasks [2, 8, 12, 26], visual search [27, 34], and scene perception tasks [26], and equating those local statistics creates visual metamers [8].

Both the V2 model and TTM are slow to converge, as they must optimize to satisfy a large number of constraints arising from the measured local texture statistics. Authors in [13], on

Original Image



TTM Foveation



FGN Foveation

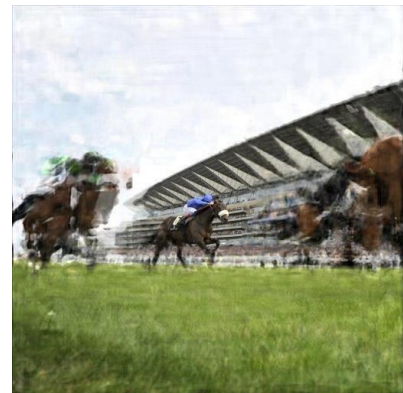


Figure 3: Four examples (rows) from the evaluation dataset showing the original image (column 1), TTM-based foveation of the image (column 2), and FGN-based foveation of the image (column 3). Unlike the deterministic radial blur function in the “Naive Foveation” section, TTM is stochastic and can generate an arbitrary number of foveated images (based on a random number generator seed) from a single source image. Therefore, one should not expect the TTM and FGN foveations to match pixel by pixel, but rather their synthesis should have similar density and type of information degradation in the periphery.

# A + BOARD

Figure 4: A classic example demonstrating the ‘‘crowding’’ effect.

the other hand, have taken a different approach to a related problem. They apply simple image distortions, such as spatial warping, to an image, and have shown that it is surprisingly difficult to tell that anything is wrong away from the fovea. Applying simple image distortions is fast to compute; however, it is not well known what distortions best capture the information available in peripheral vision; this distortion work is not yet as well grounded in terms of being able to predict task performance as TTM and the V2 model. Here the aim is to use deep networks to produce distortions like those introduced by TTM in a more computationally efficient way.

## A GENERATIVE MODEL FOR FOVEATED RENDERING

### Fully Convolutional Networks as End-to-End Generators

Researchers have long desired to speed up successful computer vision and image processing models. In many cases these successful models have taken an image as input, and mapped that image to an output image through a slow optimization process. For example, mapping from a noisy image to a denoised image. Recent advances in neural networks have provided a solution to speeding up some of these models, by learning the nonlinear mapping between the input and output images for a given model. Once learned, one can map from input to output using a relatively fast feed-forward network.

Fully convolution neural networks and other generative neural network models have been successfully used in computer vision literature for image segmentation [11, 16], deblurring [28, 29], denoising [4], inpainting [32], and super-resolution [6], artifact removal [7], and general deconvolution [33]. While many of these examples learn a mapping that removes image degradation, our work aims rather to add degradation in a way that is representative of losses in human peripheral vision. As shown in the ‘‘Human-Realistic Foveation’’ section, this is a highly nonlinear function in that the mapping changes significantly with variation in both global spatial context and in local texture statistics.

Neural networks have begun to be applied to the problem of texture synthesis, i.e. synthesizing from an example texture a new patch of perceptually similar texture. Authors in [9] use the 16 convolutional and 5 pooling layers of the VGG-19 network for texture synthesis. In the context of peripheral vision, their work could be viewed as a method for synthesizing individual pooling regions as described in the ‘‘Modeling Peripheral Vision’’ section. However, in addition to providing only a local texture synthesis, these new texture synthesis techniques have not been behaviorally validated as models of peripheral vision. Adding an behaviorally-validated, human-realistic ‘‘attentional’’ (foveation) mechanism to a generative network is a novel contributions of our work.

Given an original undistorted color image  $x_{i,j}^{\{1,2,3\}}$  of dimension  $h \times w \times 3$  and a spatial weight mask  $x_{i,j}^{\{4\}}$  of dimension  $h \times w \times 1$ , the task is to produce a foveated image,  $y$ , of dimension  $h \times w \times 3$ . The fourth channel of  $x$  captures the global spatial component of the function to be learned as it relates to the fixation point. The mask takes the form:

$$d_{i,j} = \sqrt{(i - f_y)^2 + (j - f_x)^2}$$

$$x_{i,j,4} = \begin{cases} d_{i,j}, & \text{if } d_{i,j} > d_{\text{fovea}} \\ 0, & \text{otherwise} \end{cases}$$

where  $d_{i,j}$  is the distance of each input pixel to the fixation point  $(f_x, f_y)$ , and  $d_{\text{fovea}}$  is the radius (in pixels) of the foveal region. For the results in the ‘‘Training and Evaluation of the Generative Model’’ section, the fovea radius is 64 pixels.

The proposed foveated generative network (FGN) architecture is based on several components of CNN-based deconvolution approaches [4, 7, 33] and fully convolutional segmentation approaches [11, 16]. A fully convolutional network (FCN) can operate on large image sizes and produce output of the same spatial dimensions. We extend the FCN architecture with the foveation weight mask (see above) and propagate it forward through the biases of each hidden layer in order for the spatial relation with the fixation point to be accounted for in computing the convolution and element-wise sigmoid for each layer:

$$f_k(x) = \tanh(w_k \cdot f_{k-1}(x) + b_k)$$

where  $w_k$  and  $b_k$  are the convolutions and biases at layer  $k$ , respectively.

In our implementation of FGN, there are 4 convolutional layers  $w_{1,2,3,4}$  with  $w_1$  having 256 kernels of size  $16 \times 16 \times 4$ ,  $w_2$  having 512 kernels of size  $8 \times 8 \times 256$ ,  $w_3$  having 512 kernels of size  $1 \times 1 \times 512$ , and  $w_4$  having 3 kernels of size  $8 \times 8 \times 512$ . The loss function is defined on the whole image pair  $(x, T_i(x))$  where  $T_i(x)$  is the output of the TTM model on image  $x$  given a random seed of  $i$ . For purpose of FGN, this forms a unique mapping between images, but it should be noted that TTM can generate a very large number of images  $T_i(x), \forall i \in \mathbb{N}$  for a single input image  $x$ , since the number of images that satisfy the statistical constraints imposed by the optimization in TTM are upper-bounded by an exponential function in the number image pixels.

Fig. 5 shows the fully convolutional architecture of FGN and the TTM method used to generate the foveated image pairs. The key aspect of the former is that the foveation is completed with a single pass through the network.

## TRAINING AND EVALUATION OF THE GENERATIVE MODEL

We evaluate two models of foveation. The first is a naive radial blur model known to be a poor visualization of peripheral perception as discussed in the ‘‘Introduction’’ section.

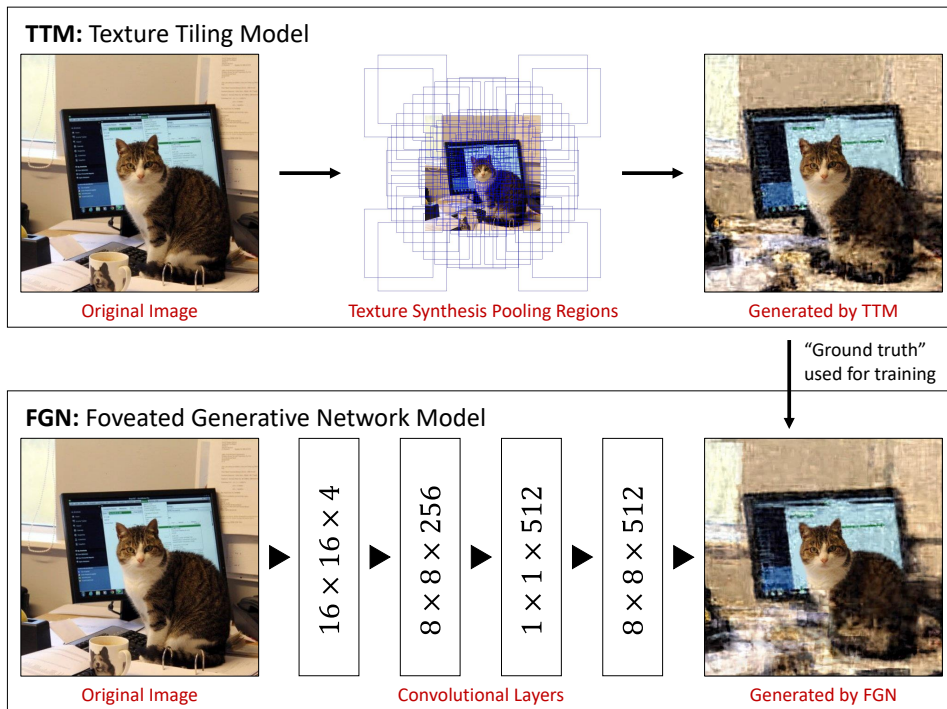


Figure 5: The architecture of the foveated generative network (FGN) used to approximate the computationally-costly texture tiling model (TTM). The output of the TTM is used as the ground truth for the end-to-end training of the FGN.

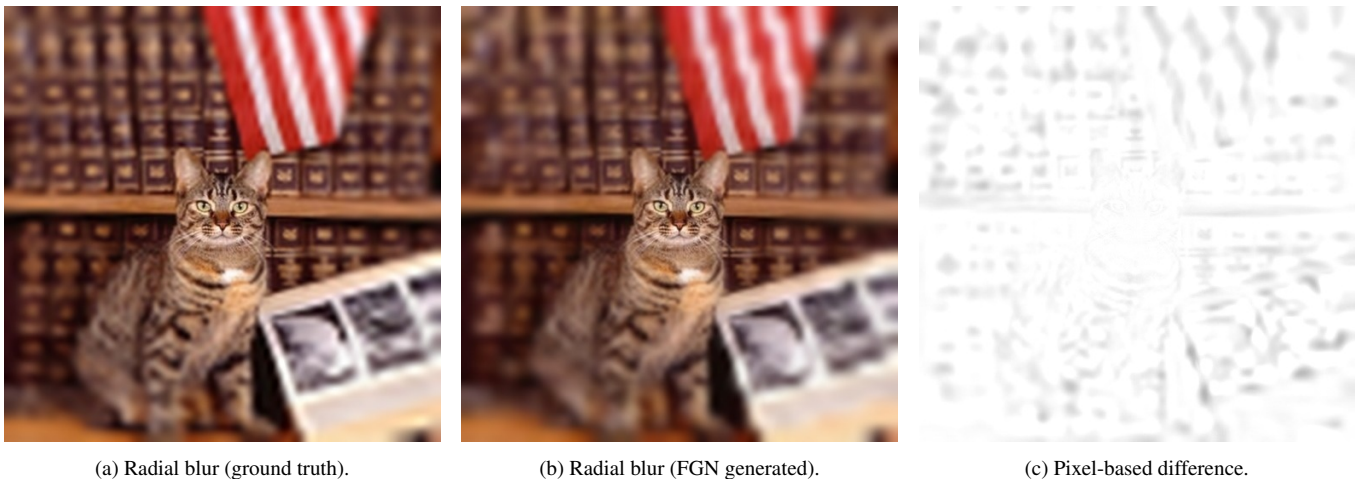


Figure 6: Example output of the radial blur computed directly (a) and learned through the FGN architecture (b). The pixel-by-pixel difference between the two images (c) shows in black the pixels of the FGN-generated image that differs from the ground truth.

However, it is a deterministic model for which there is a one-to-one mapping between source image and the ground truth. Therefore, it is a good test of whether FGN can learn a function that is spatially dependent in a global sense on the fixation point, since the pixel-wise image difference is a more reasonable metric of comparison for a deterministic model. In addition, the greater visual interpretability of the naive radial blur model allows us to gain intuition about the representation learning power of the FGN model. It’s important to empha-

size, that the radial blur is a crude model of acuity loss that cannot serve as a reasonable model of acuity loss in the periphery. In contrast to this, the second model of foveation we consider is the TTM model that has been shown in behavioral experiment to capture some of the more complex characteristics of perception in the periphery (i.e., crowding).

The original undistorted images in this paper are natural scene images selected from the Places dataset [35]. 1,000 images were selected for training the FGN on both the radial

blur model (see the “Naive Foveation” section) and the TTM model (see the “Human-Realistic Foveation” section). Another 1,000 images were used in evaluating FGN trained on both models. All images were cropped and resized down to  $512 \times 512$  pixels. For both training and quantitative evaluation, in this paper we assume a fixation at the center of the input image, i.e.  $(w/2, h/2)$ . For our application case studies (the “Application Case Studies” section), we demonstrate the ability to move the “fovea” of the trained model.

### Naive Foveation: Training on Radial Blur Model Output

In order to evaluate the ability of FGN to learn a “foveating” function, we use a Gaussian blur with the standard deviation proportional to the distance away from the fixation. The maximum standard deviation is set to 4 and decreases linearly with distance as both approach zero. Note that this blur is made greater than that needed to mimic human peripheral loss of acuity for the purpose of visualizing the effectiveness of our training procedure. Fig. 6a shows the result of applying the radial blur on one of the images from test set. This blurring function was applied to all 1,000 images in the training set and used as  $y$  in  $(x, y)$  image pairs for training an FGN network to estimate the radial blur function. Fig. 6b shows the result of running the image in Fig. 2a through the trained network, and Fig. 6c shows the difference between this generated image and the ground truth.

Since radial blur is a deterministic function, we can estimate the pixel error of the images generated by FGN. The trained model was run on each of the 1,000 images in the test set and achieved an average pixel difference of 2.3. Note that the difference shown in Fig. 6c is inverted intensity-wise for visualization clarity. This result is a quantifiable verification that FGN can learn a simple radial blurring function, and thus presumably can capture the loss of acuity in the periphery.

### Human-Realistic Foveation: Training on TTM Output

The open question asked by this paper is whether a neural network can learn to degrade peripheral information in an image in a way that is structurally similar to behaviorally validated models like TTM. The results shown for 4 images in Fig. 5 and for 1,000 foveated test images made available online at [https://\\*\\*\\*\\*.\\*\\*\\*\\*.\\*\\*\\*/peripheral](https://****.****.***/peripheral) indicate that FGN is able to capture many of the peripheral effects such as crowding and acuity loss. However, evaluating FGN’s ability to capture the degree of this degradation not as straightforward as evaluating a radial blur model. The TTM model produces multiple output images for each input image, which can look radically different while still maintaining consistent texture statistics. One does not expect the FGN output to look exactly like any given TTM output. Furthermore, peripheral vision loses substantial local phase (location) information, an effect well captured by TTM. These two factors make it impossible to evaluate FGN through pixel-based comparison with the output of TTM. We cannot simply look at the difference between the TTM image and the FGN output, as we did when evaluating radial blur. Here we show that FGN and TTM produce qualitatively similar distortions, and evaluate the degree to which the TTM and FGN outputs match on the statistics explicitly measured by TTM.

In Fig. 3, the first column has the original images, the second column has the TTM foveated images, and the third column has the FGN Foveation. Visual inspection of these images reveals several key observations. First, the fovea region with the 64 pixel radius is reproduced near-perfectly (the average pixel intensity difference is below 1.9). Second, the results capture a number of known effects of crowding, including the “jumbling” loss of position information, coupled with preservation of many basic features such as orientation and contrast, and dependence of encoding quality on local image contents, including fairly good preservation of homogeneous textured regions [14, 15, 31]. For example, the readability of text in the periphery of the second images is degraded significantly by its nonuniform positional displacement. Third, visual acuity decreases with distance from the fixation point for all 4 images.

### Statistical Validation of FGN

The FGN model was trained and evaluated based on its ability to mimic, in a meaningful statistic way, the foveated images produced by the TTM model. Therefore, statistical validation of FGN was performed by comparing its output to TTM output over the same exact pooling regions that were used for the original TTM generation process. In other words, this comparison evaluates the degree to which FGN is able to mimic the texture feature vector on a region by region basis and thereby mimic the information degradation modeled by TTM.

Fig. 7) shows the per-image difference in the feature vector representing the texture statistics in each pooling region over that image. Each bar represents a unique image. The error in each case is computed for each of the 1,000 images in the test dataset and sorted from highest (left) mean error to lowest (right). Only the highest 100 errors are shown in the figure for clarity. The mean and standard deviation of the error are computed for each image by aggregating over each of the values in the summary statistics vector in each of the pooling regions. All mean errors are below 8% for the comparison with the TTM output.

### Running Time Performance

TTM hyper-parameters were chosen such that texture synthesis convergence was achieved. For these parameters, the average running time per image was 4.2 hours. The model is implemented in Matlab and given the structure of underlying iterative optimization is not easily parallelizable.

The FGN architecture was implemented in TensorFlow [1] and evaluated using NVIDIA GTX 980Ti GPU and a 2.6GHz Intel Xeon E5-2670 processor. The average running time per image was 0.7 seconds. That is an over 21,000-fold reduction in running time for foveating an image. There are several aspects of this performance evaluation that indicate the possibility of significant further reductions in running time: (1) no code optimization or architecture pruning was performed, (2) the running time includes I/O read and write operations on a SATA SSD drive, and (3) the GPU and CPU are 2-4 years behind the top-of-the-line affordable consumer hardware.

### APPLICATION CASE STUDIES

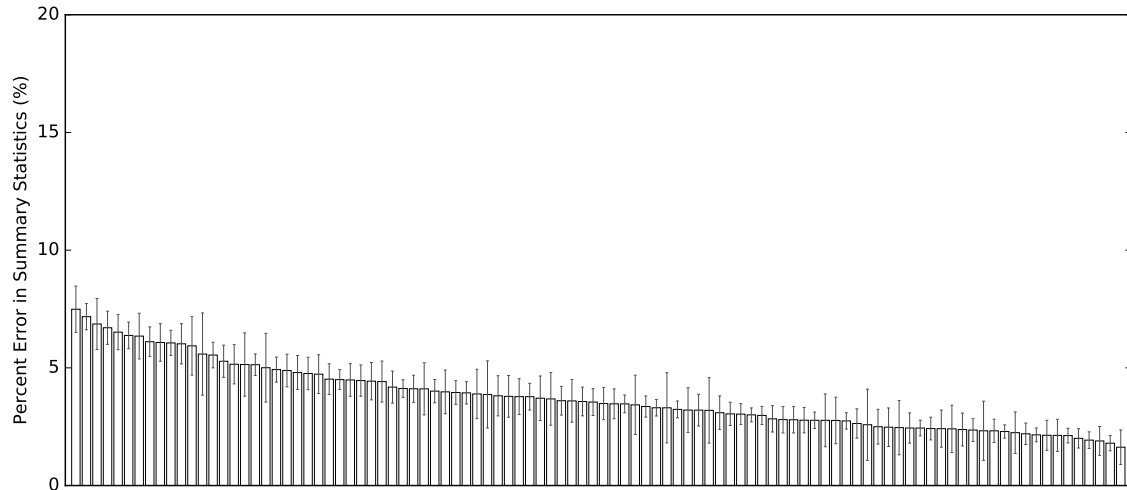


Figure 7: Percent difference (error) between FGN output and TTM output. The error is computed for each of the 1,000 images in the test dataset and sorted from highest (left) mean error to lowest (right). Only the highest 100 errors are shown in this figure for clarity. The mean and standard deviation of the error are computed for each image by aggregating over each of the values in the summary statistics vector in each of the pooling regions. All mean errors are below 8%.

Peripheral vision simulation as an approach to design is enabled by this work through the release of two things: (1) an algorithm implementation and (2) an online tool. As described in the “Running Time Performance” section, the algorithm implementation uses TensorFlow and Python, and provides a pre-trained generative network that takes an image as input and produces a foveated image as output. It also takes several parameters that specify the size and position of the fovea. These parameters control the preprocessing of the image before it is passed through the network.

The online tool (named SideEye) provides an in-browser JavaScript front-end that allows a user to load in an image that is then passed to a Linux server backend where the FGN network run inference on the image with the fovea position in each of 144 different locations (12x12 grid on an image). The result is 144 images, each foveated at grided locations. When visualized together with the SideEye tool, these images automatically foveate to the position of a hovering mouse (or, for a smartphone/tablet, the last position a finger touched the display). Two sample mouse position for a resulting foveated set are shown in Fig. 1.

Both the SideEye tool and the pre-trained FGN network can be used to perform fast peripheral vision simulation in helping understand how a user visually experiences the design under question when first glancing at it. In the follow subsections, we provide two case studies where SideEye is used to provide insight into how the design in question may appear in the periphery and what that may mean for the overall experience that the design is intended to provide.

#### Application Case Study: A/B Testing of Design Layouts

A case study of a shipping website describes a significant increase in customers requesting quotes [5] based on a redesign shown in Fig. 8. During the design process, FGN could have

been used to reveal the information available in a glance at the website. We modeled the perception of the page when the user points his eyes at the first word (“Serving”) of the most relevant content. Based on the output of FGN on the first design (Fig. 8), the model predicts that a first-time visitor may be able to recognize a truck, localize the logo, and tell that the background image contains a natural scene of some sort. Beyond that, the user might notice a black region, with blue below it, and an orange circle. The black region, at least, appears to contain some text. Furthermore, the model predicts that the user should be able to distinguish a light rectangle at the top of the page, and a darker rectangle across the middle of the page, both of which the user may guess are menu bars. This is all useful information for a user to obtain at a glance.

In the second version of the page, the model predicts that a user will easily determine that there is text against the blue background. The location of the corporate logo is now very clear, as are both of the menu bars. The blue region in the top half of the page contains a red rectangle, possibly containing some text. Higher level knowledge about web pages likely suggests that this is probably a button.

Given these FGN outputs, a designer could conclude that the button in both designs is “salient” in the sense of being an attention-getting color. However, the button is more obviously a button in the second design, even when fixating several degrees away. Given these predictions, it is perhaps no surprise that users more frequently clicked on the button to request a quote when interacting with the second design. Visualization of human perception, coupled with this kind of reasoning process may help a designer to arriving at the more effective design prior to testing with users, as described in [5].

#### Application Case Study: Logo Design Analysis



(a) Old design snapshot (original image).



(b) Old design snapshot (image foveated on “S” in “Serving”).



(c) New design snapshot (original image).



(d) New design snapshot (image foveated on “S” in “Serving”).

Figure 8: Given original images (a, c), the foveated images provides a visualization of human-realistic perception of the information available from a single glance (b, d). This particular visualization assumes that the two subfigures are 14.2 inches away from the observer on a printed page (2.6 inches in height and width) and the observer’s eyes are fixated on the “S” in “Serving” (middle left).

The ability to recognize a logo at a glance, even in the periphery, has significant potential upside for brand exposure and recall [30]. We can use peripheral vision simulation to evaluate how quickly the recognizability of a particular logo design degrades in the periphery. Understanding how the logo appears in the observer’s periphery may help understand the potential effectiveness of product placement in the physical world and in layout design on the web or on the printed page.

Fig. 9 shows the application of FGN to two versions of famous logos: (1) an earlier version of the company’s logo and (2) the current version of their logo. The left two columns show logos in their undistorted version. The right two columns visualize these logos as they may appear in the periphery when the fovea is centered at the black cross to the left of the logo in question.

Using the metric of peripheral recognition, the new Spotify, Airbnb, and Google logos appear to be an improvement, while both the new eBay and Starbucks logos appear to have a decreased recognizability in the periphery. It should be noted, that there may be other metrics under which the results are reversed, such as how memorable the logo is on repeated viewing. In that sense, peripheral vision simulation may be a useful process in a broader analysis of logo design.

## CONCLUSION

We show that a generative network with a spatial foveating component can learn in an end-to-end way to efficiently estimate the output of a human-realistic model of peripheral vision. We achieve a 4 orders-of-magnitude decrease in running time, from 4.2 hours per image to 0.7 seconds per image. This kind of jump in performance opens the door to a wide vari-

Full-Field View of Logo Designs  
Undistorted 512 x 512 Image

Peripheral View of Logo Designs  
Foveating the Left-Most Point (x=0, y=256)

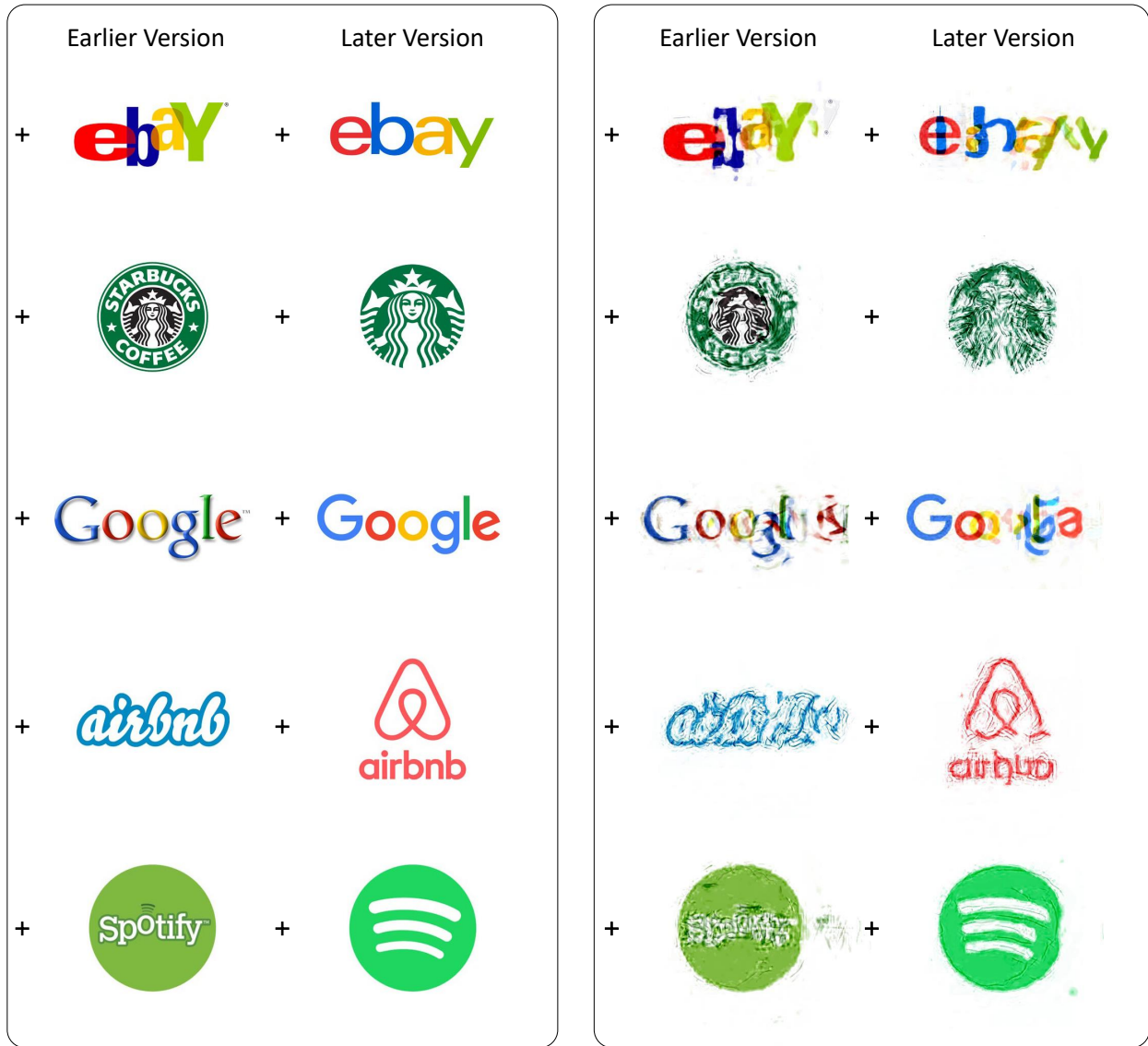


Figure 9: Visualization of how two versions of a famous brand’s logo appear in the periphery. The left two columns show the undistorted full-field views of the logos. The right two columns show peripheral visualizations of those logos when the fovea is centered on the black cross to the left of each respective logo. This kind of peripheral visualization process can be used as a tool for understanding the initial visual exposure to a design when it first appears in the observer’s periphery.

ety of applications from interface design to virtual reality to video foveation for studying human behavior and experience in real-world interactions.

*Code, Data, and Future Work*

The SideEye tool and the FGN source code are made publicly available at [https://\\*\\*\\*\\*.\\*\\*\\*.\\*\\*\\*/peripheral](https://****.***.***/peripheral). In addition, the TTM-generated images used for training are made available online. Future work will extend the size of the TTM dataset from 1,000 to 100,000 images. This will allow other

groups to propose better-performing end-to-end architectures trained on the TTM model.

## REFERENCES

1. Martin Abadi, Ashish Agarwal, Paul Barham, Eugene Brevdo, Zhifeng Chen, Craig Citro, Greg S Corrado, Andy Davis, Jeffrey Dean, Matthieu Devin, and others. 2015. TensorFlow: Large-scale machine learning on heterogeneous systems. *Software available from tensorflow.org* (2015).
2. Benjamin Balas, Lisa Nakano, and Ruth Rosenholtz. 2009. A summary-statistic representation in peripheral vision explains visual crowding. *Journal of vision* 9, 12 (2009), 13–13.
3. Herman Bouma. 1970. Interaction effects in parafoveal letter recognition. *Nature* 226 (1970), 177–178.
4. Harold C Burger, Christian J Schuler, and Stefan Harmeling. 2012. Image denoising: Can plain neural networks compete with BM3D?. In *Computer Vision and Pattern Recognition (CVPR), 2012 IEEE Conference on*. IEEE, 2392–2399.
5. Smriti Chawla. 2013. Case Study - Lead Generation Rate Shoots Up by 232% with Masthead Changes. (2013). <https://vwo.com/blog/abtesting-increases-lead-generation-rate/> [Online; accessed 10-August-2016].
6. Chao Dong, Chen Change Loy, Kaiming He, and Xiaoou Tang. 2014. Learning a deep convolutional network for image super-resolution. In *Computer Vision—ECCV 2014*. Springer, 184–199.
7. David Eigen, Dilip Krishnan, and Rob Fergus. 2013. Restoring an image taken through a window covered with dirt or rain. In *Proceedings of the IEEE International Conference on Computer Vision*. 633–640.
8. Jeremy Freeman and Eero P Simoncelli. 2011. Metamers of the ventral stream. *Nature neuroscience* 14, 9 (2011), 1195–1201.
9. Leon A Gatys, Alexander S Ecker, and Matthias Bethge. 2015. Texture synthesis and the controlled generation of natural stimuli using convolutional neural networks. *arXiv preprint arXiv:1505.07376* (2015).
10. Bruce Hanington and Bella Martin. 2012. *Universal methods of design: 100 ways to research complex problems, develop innovative ideas, and design effective solutions*. Rockport Publishers.
11. Kai Kang and Xiaogang Wang. 2014. Fully convolutional neural networks for crowd segmentation. *arXiv preprint arXiv:1411.4464* (2014).
12. Shaiyan Keshvari and Ruth Rosenholtz. 2016. Pooling of continuous features provides a unifying account of crowding. *Journal of vision* 16, 3 (2016), 39–39.
13. Jan Koenderink, Whitman Richards, and Andrea J van Doorn. 2012. Space-time disarray and visual awareness. *i-Perception* 3, 3 (2012), 159–165.
14. Jerome Y Lettvin. 1976. On seeing sidelong. *The Sciences* 16, 4 (1976), 10–20.
15. Dennis M Levi. 2008. Crowding - An essential bottleneck for object recognition: A mini-review. *Vision research* 48, 5 (2008), 635–654.
16. Jonathan Long, Evan Shelhamer, and Trevor Darrell. 2015. Fully convolutional networks for semantic segmentation. In *Proceedings of the IEEE Conference on Computer Vision and Pattern Recognition*. 3431–3440.
17. Laura Parkes, Jennifer Lund, Alessandra Angelucci, Joshua A Solomon, and Michael Morgan. 2001. Compulsory averaging of crowded orientation signals in human vision. *Nature neuroscience* 4, 7 (2001), 739–744.
18. Denis G Pelli, Najib J Majaj, Noah Raizman, Christopher J Christian, Edward Kim, and Melanie C Palomares. 2009. Grouping in object recognition: The role of a Gestalt law in letter identification. *Cognitive Neuropsychology* 26, 1 (2009), 36–49.
19. Denis G Pelli, Melanie Palomares, and Najib J Majaj. 2004. Crowding is unlike ordinary masking: Distinguishing feature integration from detection. *Journal of vision* 4, 12 (2004), 12–12.
20. Denis G Pelli and Katharine A Tillman. 2008. The uncrowded window of object recognition. *Nature neuroscience* 11, 10 (2008), 1129–1135.
21. Javier Portilla and Eero P Simoncelli. 2000. A parametric texture model based on joint statistics of complex wavelet coefficients. *International Journal of Computer Vision* 40, 1 (2000), 49–70.
22. Martin Rolfs, Donatas Jonikaitis, Heiner Deubel, and Patrick Cavanagh. 2011. Predictive remapping of attention across eye movements. *Nature neuroscience* 14, 2 (2011), 252–256.
23. Ruth Rosenholtz. 2011. What your visual system sees where you are not looking.. In *Human vision and electronic imaging*. 786510.
24. Ruth Rosenholtz. 2016. Capabilities and Limitations of Peripheral Vision. *Annual Review of Vision Science* 2, 1 (2016).
25. Ruth Rosenholtz, Amal Dorai, and Rosalind Freeman. 2011. Do predictions of visual perception aid design? *ACM Transactions on Applied Perception (TAP)* 8, 2 (2011), 12.
26. Ruth Rosenholtz, Jie Huang, and Krista A Ehinger. 2012a. Rethinking the role of top-down attention in vision: effects attributable to a lossy representation in peripheral vision. *Frontiers in Psychology* (2012).
27. Ruth Rosenholtz, Jie Huang, Alvin Raj, Benjamin J Balas, and Livia Ilie. 2012b. A summary statistic representation in peripheral vision explains visual search. *Journal of Vision* 12, 4 (2012), 14–14.
28. Christian J Schuler, Michael Hirsch, Stefan Harmeling, and Bernhard Schölkopf. 2014. Learning to deblur. *arXiv preprint arXiv:1406.7444* (2014).

29. Jian Sun, Wenfei Cao, Zongben Xu, and Jean Ponce. 2015. Learning a convolutional neural network for non-uniform motion blur removal. In *Computer Vision and Pattern Recognition (CVPR), 2015 IEEE Conference on*. IEEE, 769–777.
30. Bo van Grinsven and Enny Das. 2016. Logo design in marketing communications: Brand logo complexity moderates exposure effects on brand recognition and brand attitude. *Journal of Marketing Communications* 22, 3 (2016), 256–270.
31. David Whitney and Dennis M Levi. 2011. Visual crowding: A fundamental limit on conscious perception and object recognition. *Trends in cognitive sciences* 15, 4 (2011), 160–168.
32. Junyuan Xie, Linli Xu, and Enhong Chen. 2012. Image denoising and inpainting with deep neural networks. In *Advances in Neural Information Processing Systems*. 341–349.
33. Li Xu, Jimmy SJ Ren, Ce Liu, and Jiaya Jia. 2014. Deep convolutional neural network for image deconvolution. In *Advances in Neural Information Processing Systems*. 1790–1798.
34. Xuetao Zhang, Jie Huang, Serap Yigit-Elliott, and Ruth Rosenholtz. 2015. Cube search, revisited. *Journal of vision* 15, 3 (2015), 9–9.
35. Bolei Zhou, Agata Lapedriza, Jianxiong Xiao, Antonio Torralba, and Aude Oliva. 2014. Learning deep features for scene recognition using places database. In *Advances in neural information processing systems*. 487–495.